Spectroscopy between parabolic states in hydrogen: Enhancement of the Stark-induced resonances in its photoionization

Wallace L. Glab,* K. Ng, Decheng Yao,† and Munir H. Nayfeh
Department of Physics, University of Illinois at Urbana–Champaign, 1110 West Green Street, Urbana, Illinois 61801
(Received 10 September 1984)

We present calculations of the photoionization spectrum of excited hydrogen using π polarization in the presence of a strong electric field as a function of the spherical (applicable to complex atoms) and parabolic quantum numbers of the excited state. We also present corresponding measurements of the photoionization yield from the individual parabolic states of $n=2$. Both the calculations and the measurements show an enhancement of the depth of the so-called "Stark-induced modulation" in the region $E \gtrsim 0$ when the initial excited state is a pure $m_l=0$ blue state, and disappear almost completely when the initial state is a pure $m_l=0$ red state. These results are understood using arguments based on the fact that the charge distribution of the Stark-induced states is tremendously extended up field. Because of the excellent signal to noise ratio of the enhanced modulations, we were able to measure the field dependence of the spacings with sufficient accuracy to confirm the $\frac{3}{4}$ power law and rule out the recently suggested $\frac{2}{3}$ power law.

I. INTRODUCTION

The simplest atom, the hydrogen atom, has been the subject of continuing interest to atomic physicists. This interest stems from the fact that the absence of electronic core effects allows precise calculations to be made of its properties, both in isolation and under the influence of external forces due to electromagnetic fields and collisions. This paper deals with an experimental situation which can only be found in hydrogen: spectroscopy from pure parabolic states in the presence of external electric fields. The splitting of the various fine-structure states is less than a fraction of a wave number, with the largest being 0.365 cm^{-1} occurring in $n=2$. At 475 V/cm, the Stark effect and the Lamb shift in $n=2$ become comparable, whereas at $\sim$2.910 kV/cm the Stark effect becomes comparable to the fine-structure splitting. For fields greater than about 5 kV/cm, the interaction with the Stark field dominates the fine structure, thus leading to a linear Stark splitting of $n=2$. Consequently, at these high field values pure parabolic (Stark) states can be prepared if selective narrow-band sources of excitation are available.

In complex atoms, the interaction of the outer electron with the core results in much larger splittings of the various components, thus making the field strength necessary to achieve pure Stark states in low-lying excited states very high and experimentally not feasible to apply because of breakdown. Of course, the required field strength drops for high-lying excited states. Unfortunately, the wavelengths needed for studies for the photoionization near threshold of these states are out of the range of the convenient optical and infrared tunable sources.

In the presence of large electric fields, the field induces relatively long-lived parabolic states (so-called Stark-induced resonances) in the photoionization of the atom in the region $E>0$. Each of these states is a superposition of a few parabolic states with intensity ratios typically as 0.9, 0.06, 0.02, etc. Thus, they are approximately 90% pure parabolic states.[1,2] Therefore, the capability of producing pure parabolic excited states as initial low-lying states offers the possibility of spectroscopy between them and the higher parabolic states. Previously pure parabolic states in hydrogen were prepared in states of high principle quantum number after charge exchange of a beam of protons in a rare gas.[3] All but the specific Stark state sought were quenched using microwave cavities. Transitions to higher levels at infrared wavelengths were induced using Doppler tuning. This technique in the presence of an electric field has been used to measure the energies and field ionization rates of some excited Stark states of hydrogen. However, application of this method to the states in the region near $E=0$ would be very difficult, since it would require a powerful, broadly tunable laser in the infrared; currently, such lasers are unavailable.

Recently, we made the first observation of the Stark-induced resonances in hydrogen near $E=0$.[4] Similar observation was also achieved.[5] In this paper we study excitations from parabolic (Stark) states in a given low-lying n state in hydrogen to the highly excited states near $E=0$ in the presence of a strong electric field. We present calculations of the photoionization cross section as a function of the spherical quantum numbers n and l of the initial state and as a function of the parabolic quantum numbers n_1, n_2, and m_l of that state. We give the dependence of the depth of the Stark-induced modulation on these quantum numbers, and on the electric field. Although excitation from spherical states in the presence of strong fields is not applicable to hydrogen, however, it is applicable to excitation in complex atoms.

The calculations are compared to experimental results in the case of $n=2$ in the presence of 16.9, 14, 8, 6.5 and 4.5 kV/cm. Both the calculation and the measurement

show, in agreement, an enhancement of the depth of the Stark-induced resonances in the region $E \geq 0$ when excited from a blue $m_l=0$ state. These observations are understood from arguments that are based on the fact that the electric field extends the electronic charge distribution to the broad resonances up field.

II. THEORY OF STARK EFFECT NEAR $E=0$

Several quantum-mechanical numerical calculations have been performed on the effects of a strong electric field on the highly excited states of atomic hydrogen. The calculation of Damburg and Kolosov[6] was concerned with the positions and ionization rates of the states in the combined potential, and did not address the problem of calculating excitation probabilities. Luc-Koenig and Bachelier[7] calculated photoionization cross sections for hydrogen in an electric field, but treated only excitation from the ground state. Harmin's numerical WKB calculation found the cross sections for some excited hydrogenic states; however, since the calculation was performed with a later application to complex atoms in mind, the initial states used were good states of angular momentum (for example, the $3p$ state).[2] Since detailed comparison with the experiment to be described will require the determination of the cross sections for photoionization from the $n=2$ Stark excited states, the need for a new calculation was seen.

The starting point for the calculation of the photoionization cross section of atomic hydrogen in an electric field is equations

$$\left[-\frac{1}{2}\frac{d^2}{d\xi^2}+\left[-\frac{Z_1}{2\xi}+\frac{m_l^2-1}{8\xi^2}+\tfrac{1}{8}F\xi\right]\right]\chi_1=\frac{E}{4}\chi_1\,, \quad (1)$$

$$\left[-\frac{1}{2}\frac{d^2}{d\eta^2}+\left[-\frac{Z_2}{2\eta}+\frac{m_l^2-1}{8\eta^2}-\tfrac{1}{8}F\eta\right]\right]\chi_2=\frac{E}{4}\chi_2\,. \quad (2)$$

These equations are of the form of effective one-dimensional Schrödinger equations in the coordinates ξ and η, with the separation parameters Z_1 and Z_2 playing the role of effective Coulomb charges for the motions in each coordinate. The equations are coupled through the relation $Z_1+Z_2=1$. Clearly, these potentials will depend on the azimuthal quantum number m_l and the values of Z_1 and Z_2 for the state under consideration. In order to apply WKB techniques to this problem, the Langer correction must be made: this results in the conversion of the numerators in the centripetal terms of the potentials from m_l^2-1 to m_l^2. This correction is analogous to the conversion $1(1+1)\rightarrow(1+1/2)^2$ in the field-free hydrogen atom problem. We study here the $m_l=0$ case.

We first consider the motion in the ξ coordinate. Since the motion in ξ becomes classically disallowed for ξ greater than the turning point

$$\xi_1=E/F+[(E/F)^2+4Z_1/F]^{1/2} \quad (3)$$

and remains so for all larger values of the coordinate, the magnitude of the wave function $\chi_1(\xi)$ must vanish at large values of ξ. In addition, the small-coordinate behavior of Eq. (1) causes $\chi_1(\xi)$ to be proportional to $\xi^{1/2}$ for small ξ. At a given value of energy E and field F, these conditions lead to a set of discrete eigenvalues for the separation parameter Z_1 (the effective Coulomb charge) corresponding to well-behaved wave functions.

The wave function in ξ for given values of E, F, and Z_1 is calculated by matching power-series expansions of the solution at a large number of values of the coordinate, in a technique similar to that of Damburg and Kolosov.[5] The wave function is first expanded about the origin using a power series of the form

$$\chi_1(\xi)=\xi^{1/2}\sum_{n=0}^{\infty}C_n\xi^n\,. \quad (4)$$

The small-coordinate boundary condition is explicitly displayed in this expansion. A recursion relation for the coefficients C_n is obtained by substitution of this expansion into Eq. (1), yielding

$$C_n=\frac{1}{n^2}(-Z_1C_{n-1}-\tfrac{1}{2}EC_{n-2}+\tfrac{1}{4}FC_{n-3})\,. \quad (5)$$

The resulting expansion converges for all ξ, but in practice it is impossible to calculate terms of high enough order to give accurate values for the wave function over the entire region of interest. For this reason, this series is carried to only 20 terms and is used to calculate the solution and its slope at a small value of $\xi_0=0.01$ a.u. The wave function is then expanded about this value of the coordinate in a new power series in $(\xi-\xi_0)$ which is matched in magnitude and slope to the previously calculated function.

Substituting the following power-series form

$$\chi_1(\xi)=\sum_{n=0}^{\infty}C_n^{(i)}(\xi-\xi_i)^n \quad (6)$$

into Eq. (1) yields a recursion relation for the coefficients of an expansion about any value of the coordinate ξ_i:

$$C_n^{(i)}=\frac{-1}{\xi_i^2n(n-1)}\left[2\xi_i(n-1)(n-2)C_{n-1}+\left[\tfrac{1}{4}+(n-2)(n-3)+Z_1\xi_i+\frac{E}{2}\xi_i^2-\frac{F}{4}\xi_i^3\right]C_{n-2}\right.$$
$$\left.+\left[Z_1+E\xi_i-\frac{3F}{4}\xi_i^2\right]C_{n-3}+\left[\frac{E}{2}-\frac{3F}{4}\xi_i\right]C_{n-4}-\frac{F}{4}C_{n-5}\right]\,. \quad (7)$$

This series converges for $\xi-\xi_i<\xi_i$; therefore, this expression can be used to calculate the wave function using a limited number of terms for values of $\xi-\xi_i$ which are a small fraction of ξ_i. This expansion is used to calculate χ_1 and $d\chi_1/d\xi$ at a new, larger value of the coordinate ξ_i such that $\xi_i-\xi_{i-1}\ll\xi_i$.

At each new value of ξ_i the wave function is expanded and matched to the previous expansion, and then used to

calculate the value and slope at the point of the next expansion. The size of the steps in the coordinate must be chosen to be small enough that the series will converge using a small number of terms (20) and the solution will not vary much over the interval (to facilitate subsequent numerical integration), but not so small as to lead to excessive calculation times. Since the wave function varies rapidly near the origin and more slowly as ξ increases, the size of the steps in ξ were chosen to make an exponential approach to a constant step size S_0 as a function of ξ,

$$S = S_0[1-\exp(-\xi/\xi_0)] . \tag{8}$$

For $S_0/\xi_0 \ll 1$, rapid convergence of the series expansions is assured. The values of S_0 and ξ_0 are chosen to keep the total number of expansion points reasonable while ensuring that the solution does not vary much between successive steps.

The numerical calculation of $\chi_1(\xi)$ is continued using this procedure to a value of ξ considerably greater than the classical turning point. In this way the solution is generated for a given E, F, and Z_1. In order to find the eigenvalues for an energy and field value, the following procedure is used. The wave function is first calculated for $Z_1=1$, and the value of the wave function at the end point is stored. The value of Z_1 is then decremented by a small amount and the value of the wave function is recalculated, stored, and compared to the original value. Z_1 is decremented until the value of the solution at the endpoint changes sign; when this occurs, Z_1 is changed by a smaller amount in the opposite sense. In this manner the program iterates through values of Z_1, searching for a value at which the wave function vanishes. Convergence of Z_1 to an eigenvalue to a precision of $\sim 10^{-9}$ occurs within about 30 iterations. The calculated eigenvalues are insensitive to variation of the value of the endpoint if it is chosen to be more than about twice the value of the classical turning point. On the final iteration, the values of the coordinate and the wave function for each step are stored for use in later computation.

Once an eigenvalue has been found for a given E and F, the condition $Z_1+Z_2=1$ gives the value of Z_2, allowing numerical calculation of the wave function in the coordinate η from Eq. (2). This calculation is performed in the same way as that for the ξ wave function; however, the coefficients differ in that $Z_1 \rightarrow Z_2$ and $F \rightarrow -F$.

The wave function $\chi_2(\eta)$ has the same behavior for small coordinate values as $\chi_1(\eta)$ but is unbound for all energies if the electric field magnitude is nonzero. Thus, at large values of η it has an oscillatory character; asymptotically, the time-independent wave function has the form

$$\chi_2(\eta) = \frac{2A}{\sqrt{\pi}} \frac{1}{F^{1/4}} \frac{1}{(\eta+2E/F)^{1/4}} \times \sin\left\{\left[\frac{\sqrt{F}}{3}\left[\eta+\frac{2E}{F}\right]^{3/2}\right]+\delta\right\} . \tag{9}$$

The quantities A and δ are found by calculating the slope and magnitude of the wave function at some distant point and substituting these values into corresponding expression derived from the asymptotic form, which gives A and δ in terms of these quantities. The calculated values of $\chi_2(\eta)$ are stored in an array along with the values of η. Since the full wave function of the system is

$$\psi = \frac{1}{\sqrt{\xi\eta}} \chi_1(\xi)\chi_2(\eta) e^{im_l\phi} \tag{10}$$

the program has at this point produced a numerical solution proportional to the true wave function corresponding to the calculated eigenvalue Z_1, for a given E and F.

In order to calculate the excitation matrix elements, the numerical wave function must be normalized. As is typical for continuum state wave functions, normalization is done per unit energy interval,

$$\int \psi^*(Z_1,E)\psi(Z_1',E')dV = \delta_{Z_1,Z_1'}\delta(E-E') , \tag{11}$$

where $dV=(\xi+\eta/4)d\xi\, d\eta\, d\phi$ in parabolic coordinates. This normalization condition can be shown to be equivalent to setting the outgoing flux from the atom equal to unity. Writing the normalized wave function as

$$\psi_{\text{norm}} = \frac{(C_{Z_1,E})^{1/2}}{\sqrt{\xi\eta}} \chi_1(\xi)\chi_2(\eta) e^{im_l\phi} , \tag{12}$$

a calculation of the outgoing flux yields the normalization constant for the numerical wave functions,

$$C_{Z_1,E} = \left[A^2 \int_0^\infty \frac{\chi_1(\xi)}{\xi} d\xi\right]^{-1} . \tag{13}$$

The integral is computed by Simpson's rule during the final iteration of the calculation of $\chi_1(\xi)$; using this quantity and the value of A found earlier, the normalization constant is found. The values of the integral and A are not sensitive to changes in the step sizes (within reason), and A is insensitive to the exact value of the distant point at which it is calculated, as long as the asymptotic form of $\chi_2(\eta)$ is valid at that point. Comparison of some results of this calculation modified to work at zero field to the well-known analytic forms of the solutions in parabolic coordinates has shown these wave functions to have a relative accuracy of about 10^{-5}.

The photoionization cross section for π excitation can be written using parabolic coordinate wave functions as

$$\sigma(E) = \sum_{n_1}^{\infty} \delta(n_1,E) 4\pi^2\alpha(\hbar\omega) \sum_{n_1}^{\infty} |\langle \psi_f(n_1,E)|z|\psi_i\rangle|^2 . \tag{14}$$

As noted earlier, only final states with $0 \le Z_1 \le 1$ will contribute significantly to the cross section. Calculation of the cross section therefore requires the determination of the eigenvalues Z_1 within this range and the corresponding final state wave functions, followed by calculation of the matrix elements. Once the matrix elements have been found, the partial cross sections $\sigma(n_1,E)$ and the total cross section $\sigma(E)$ can be calculated.

Since the initial states of interest are low lying, they are essentially unaffected by the electric field. Therefore, the matrix elements may be computed using the zero-field analytic expression for the initial state under consideration. The z matrix element in parabolic coordinates is

$$\langle \psi_f(n_1,E) \mid z \mid \psi_i \rangle = \frac{\pi}{4} \int \psi_f(n_1,E)(\xi^2-\eta^2)\psi_i \, d\xi \, d\eta \ . \tag{15}$$

This two-dimensional integral is calculated using Simpson's rule over the same variable steps in ξ and η used in the calculation of the wave functions. The partial cross section is then calculated for this eigenvalue using this result, and the process is repeated for each of the calculated eigenvalues. Finally, the photoionization cross section for the value of energy and field under consideration is found by taking the sum of the partial cross sections. In addition, the program calculates the quantum number n_1 for the state responsible for each partial cross section, allowing the states leading to structure in the photoionization to be identified.

The resulting cross sections have been tested for their sensitivity to variations in the various parameters of the calculation such as number of expansion terms retained, step size function and end points of calculation, and are believed to have a relative accuracy of about 10^{-3}. As an additional check, the transition rates between analytically calculated $n=2$ states and numerically calculated $n=3$ states were found. These rates were in agreement with zero-field theory to an accuracy greater than that stated above.

The modulations at $E=0$ at 16.5 kV/cm for the ground state, the $n=2$ states, 100 and 010 states, and for the $n=3$ states 200, 110, and 020 are presented in Table I. Moreover, the results for excitation from some spherical states are shown in the same table. Here the modulation is defined as the difference between the cross sections at the maximum and minimum of the resonance divided by the average value. These results show that for the 100 initial state the predicted depth of modulation is more than twice that for the ground state, while that for the 010 state is so small as to be practically unobservable. The situation is even more pronounced for the $n=3$ states.

Comparison between excitation from spherical and parabolic states is also interesting since the spherical case is applicable to excitation in complex atoms. Our results in Table I show that for excitation from the ground states both cases give essentially the same result. However, for excitation from excited states we have drastic differences between the two cases. We find an enhancement of the depth of the Stark-induced modulation in the region $E \geq 0$ when the initial excited state is a pure $m_l=0$ blue state, and disappear almost completely when the initial state is a pure $m_l=0$ red state.

III. EXPERIMENTAL

We now discuss the experimental test of these calculations. The experimental apparatus was described previously.[4,8] Here we only describe it briefly. The technique we use utilizes the simultaneous absorption of two photons from a single tunable pulsed laser beam at 243 nm resulting in excitation from $1s$ to $n=2$, and some photoionization of the resulting $n=2$ population. A second pulsed beam at $\sim$366 nm excites states near the continuum from the $n=2$ state. The atomic hydrogen source is a modified Wood discharge tube. An atomic beam is formed by effusion from the discharge region through a multicollimator assembly. The atomic beam is directed into the diffusion pumped cell which contains the field plates. The beam is loosely collimated, but produces a density of about 10^{11} H^0/cm^3; the background gas density is on the order of $10^{12}/cm^3$. Ions produced by the laser radiations are driven by the electric field through a grid in the grounded plate. They travel through a 1-m-long, field-free drift tube which provides mass analysis. This is necessary since molecular impurities are easily ionized by the ultraviolet wavelengths in use. Ions are detected using an 18-stage venetian blind electron multiplier capable of single ion detection. Under typical experimental conditions, several hundred ions are detected per pulse. The data are collected and analyzed using a Digital Equipment Corporation LSI-11/23 minicomputer system.

The optical beams needed for the excitation of atomic hydrogen are produced using a pulsed laser system: an Nd^{+3}:YAG laser and two dye lasers. A fraction of the second harmonic of the YAG laser at 532 nm is used to pump one of the dye lasers producing a beam at 630 nm, which is frequency doubled to 315 nm by a KDP crystal and then summed with the residual YAG fundamental by a KDP crystal resulting in a beam at 243 nm of pulse length of about 15 ns, a bandwidth of about 1.5 cm^{-1}, and pulse energies on the order of 10 microjoules. The second dye laser produces a beam at about 555 nm which is summed with part of the YAG fundamental to produce a beam with pulse length near 10 ns, bandwidth of 0.6 cm^{-1}, pulse energies of a few tenths of a millijoule and wavelength near 365 nm.

IV. PREPARATION OF PARABOLIC STATES OF H($n=2$) STATE

The feasibility of producing pure parabolic states in $n=2$ hydrogen state is now described. Since we are in-

TABLE I. Effect of initial state on the depth of the Stark-induced resonances.

	Parabolic states (n_1,n_2,n)					
n	n_1	n_2	m_l	%	Spherical states	%
1	1	0	0	20.4	$1s$	20.4
2	1	0	0	57	$2s$	20.4
	0	1	0	2.3	$2p$	38
3	2	0	0	89.7	$3s$	18.8
	0	2	0	0.3	$3p$	39.6
	1	1	0	11.0		
4	3	0	0	123.9		

terested in applying fields larger than 2 kV/cm, we will not include the Lamb shift in our analysis since, as we mentioned above, the Stark shift becomes comparable to it at ~ 0.475 kV/cm. In the region of 2–5 kV/cm the calculations of the $n=2$ Stark effect are quite complicated. Only n and m_j are good quantum numbers, but neither j and l, nor the parabolic quantum numbers are. At fields higher than 5 kV/cm, the interaction with the Stark field dominates over the fine structure, thus leading to a linear Stark splitting; consequently, the states can have good parabolic quantum numbers. Such calculations were previously done for $n=2$, 3 and 4.[9] In Lüder's treatment the Hamiltonian matrix for the $n=2$, $m_j=\frac{1}{2}$ states interacting with an electric field is calculated, with the result

$$\hat{H}=\begin{array}{c} \begin{matrix} 2p_{3/2} & 2p_{1/2} & 2s_{1/2} \end{matrix} \\ \begin{pmatrix} 0 & 0 & A\sqrt{6} \\ 0 & -\frac{1}{16} & -A\sqrt{3} \\ A\sqrt{6} & -A\sqrt{3} & -\frac{1}{16} \end{pmatrix} \end{array} \begin{matrix} 2p_{3/2} \\ 2p_{1/2} \\ 2s \end{matrix},$$

where $A=ea_0F/\alpha^2(\mathrm{Ry})$ in cgs units where Ry is the Rydberg energy, and the zero of energy is taken to be that of the field-free $2p_{3/2}$ level. This matrix is diagonalized, leading to a secular equation for the energy eigenvalues

$$\xi^3+\tfrac{1}{8}\xi^2+(\tfrac{1}{256}-9A^2)\xi-\tfrac{3}{8}A^2=0\,,$$

where $\xi=\Delta E/\alpha^2(\mathrm{Ry})$. Solution of the secular equation gives the energy shifts of the states, allowing the calculation of the eigenvectors as coherent superpositions of the zero-field states. The overlaps of these states with the pure parabolic states 100, 010, and 001 can then be easily found, giving the probability amplitudes for the parabolic state superpositions comprising each Stark state for a given field. Here we present numerical results based on these calculations relevant to our method of excitation of $n=2$, namely, two-photon process using π polarization radiation.

Figure 1 gives the Stark splitting of $n=2$ as a function

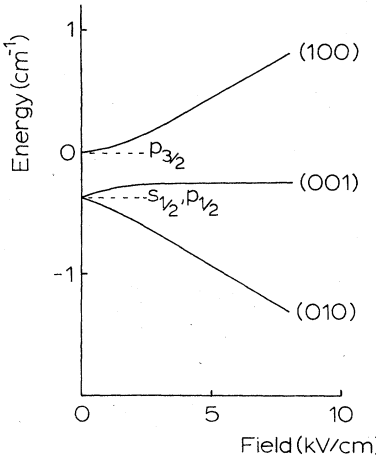

FIG. 1. Calculated Stark splittings of the $n=2$ state of hydrogen as a function of the applied electric field. The Lamb shift is neglected, and the states are labeled at high fields by their parabolic quantum numbers.

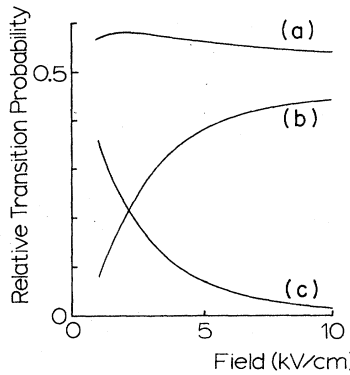

FIG. 2. The calculated absolute percentage of the various m_l states excited from the ground state of hydrogen using a two-photon process as a function of the applied electric field. The polarization of the radiation is parallel to the field (π polarization) and the bandwidth is larger than the Stark splittings.

of the electric field. At higher fields the states are labeled by their parabolic quantum numbers $(n_1,n_2,|m_l|)$. The state (100) originating from $p_{3/2}$ is what we call the $m_l=0$ blue state, whereas the state (010) originating from $p_{1/2},s_{1/2}$ is what we call the $m_l=0$ red state. The $|m_l|=1$ state is the least shifted state.

We will now discuss the efficiency of populating the various Stark states of $n=2$ using the two-photon (π polarization) process. Two cases will be discussed. In the first the laser bandwidth is wide enough such that the Stark states cannot be resolved, hence they are excited simultaneously. In the second the bandwidth is narrow enough such that individual components can be excited. Figure 2 gives the percentage of population of the $|m_l|=1, m_l=0$ blue state and $m_l=0$ red state as a function of the electric field ($F\geq 1$ kV/cm) assuming the states are not resolved. It is known that in the zero-field limit $|m_l|=1$ state is not excited in the $\pi-\pi$ excitation. The presence of a field of 3 kV/cm produces about 30%,

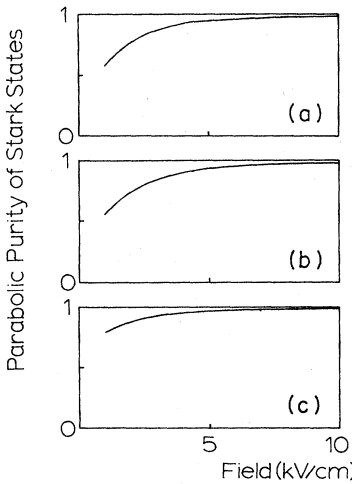

FIG. 3. The purity of the blue-shifted (a), unshifted (b), and red-shifted (c) Stark states as a function of the electric field, in terms of the parabolic states to which they tend at high field.

however, at high fields (>15 kV/cm) this population drops to less than a few percent. We also note that the two $m_l=0$ states approach 50 percent populations at higher fields with the red one approaching faster than the blue one.

Figure 3 gives the percentage of purity of the various states if each state is selectively excited by radiation whose effective bandwidth is less than the splittings. Above 10 kV/cm both of the $m_l=0$ states can be purely excited ($>97\%$) whereas the $|m_l|=1$ state is not excitable. Thus, in principle, with fields larger than 8 kV/cm, excitation of pure parabolic states of $n=2$ in hydrogen can be achieved. But because our laser bandwidth is ~ 1.5 cm^{-1}, then in practice we can only excite pure states using fields larger than 10 kV/cm such that the Stark splitting is larger than 3 cm^{-1}. Since we use quite low atomic hydrogen density, we find no problem in dropping up to 18 kV/cm across our interaction region; thus making these kinds of studies feasible.

V. EXPERIMENTAL RESULTS AND ANALYSIS

Figure 4 gives the ionization spectrum at field values 4.5, 6.5, and 8 kV/cm. The 243-nm beam is of π polarization and does not resolve the Stark splittings. The ionization beam is tuned across the $E=0$ region and is also of π polarization.

Figure 5 was taken at higher fields where the Stark splitting is large enough to allow selective excitation of the parabolic states. In Fig. 5(a), the 243-nm beam was selectively exciting the $m_l=0$ blue state, whereas in Fig. 5(b) the $m_l=0$ red state was selectively excited.

These observations can be understood from the following arguments that are based on the charge distribution of the broad resonances, and that of the parabolic states of $n=2$ state. From the Stark theory it is known that the electronic charge distribution of the broad resonances is

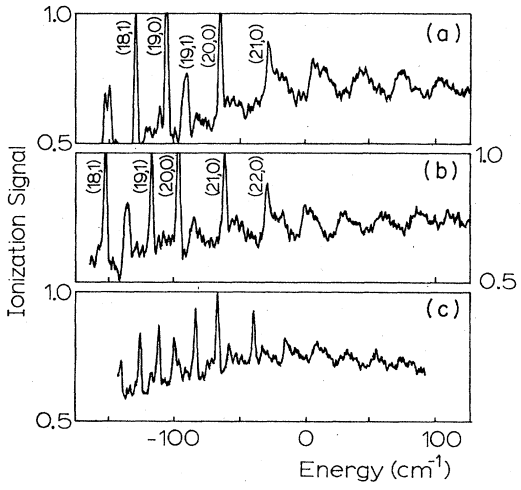

FIG. 4. The photoionization spectrum of hydrogen near the field-free photoionization threshold $E=0$ in the presence of three different Stark fields (a) 8.0, (b) 6.5, (c) 4.5 both light beams have π polarization. Some quasidiscrete states are labeled by (n_1,n_2). All states are $m_l=0$.

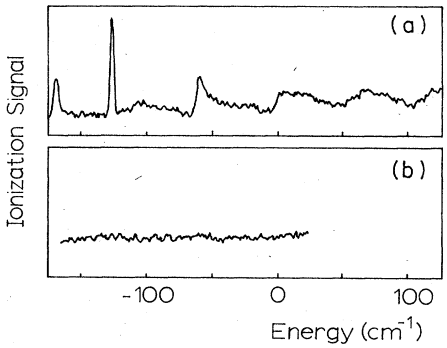

FIG. 5. The photoionization spectrum of ground state hydrogen near $E=0$ in the presence of 16.9 kV/cm. Both beams have π polarization. The 243-nm beam is selectively exciting the (a) $m_l=0$ blue state of $n=2$ (100) and (b) $m_l=0$ red state of $n=2$ (010).

highly polarized along the axis of the electric field and predominately up field with respect to the nucleus. On the other hand, each Stark state of $n=2$ state has a different charge distribution. In fact, there is a correlation between the energy shift and this distribution. As the shift increases, the charge distribution gets more and more concentrated along the field, being mostly up field if the shift is positive (blue states) and down field if the shift is negative (red states).

Using these arguments, one therefore expects to have a large overlap between the wave function of the $m_l=0$ blue state of $n=2$ and that of a broad resonance because both distributions are elongated up field. On the other hand, we expect much reduced overlap between the wave functions of the $m_l=0$ red state and a broad resonance. These conclusions are precisely what causes the disappearance of the modulation when we use the $m_l=0$ red state as an initial state. In fact, the disappearance of the modulation in Fig. 5(b) is accompanied by an enhancement of their depth in Fig. 5(a) taken with the blue Stark state as an initial state.

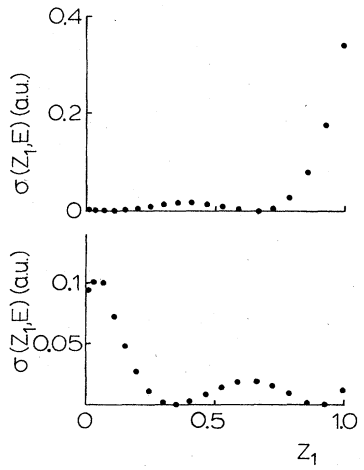

FIG. 6. The distributions of partial photoionization cross sections for the $n=2$, $m_l=0$ parabolic states, (a) is for the blue-shifted 100 state, while (b) is for the red-shifted 010 state.

These conclusions can now be quantitatively supported by examining the partial cross sections for different values of Z_1. At a given energy and field, a finite number of Z_1 eigenvalues fall within the range $0 \leq Z_1 \leq 1$, each of which corresponds to a state with quantum number n_1. As the energy of the highly excited states increases, thresholds for the excitation of states of higher n_1 are reached. In terms of Z_1, these thresholds are those energies for which an eigenvalue of $Z_1 = 1$ occurs. Figures 6(a) and 6(b) show the distributions for excitation by π polarized light from the blue-shifted 100 state and the red-shifted 010 state to near $E=0$ for $F=16.5$ kV/cm, respectively. The important feature of these distributions is the large enhancement of the partial cross section of the $Z_1 \sim 1$ state from the 100 state relative to the redder states. For the 010 initial state, the redder states which contribute to the smooth background have the larger cross sections. Thus the blue-shifted 100 state has a large excitation probability to blue-shifted final states ($Z_1 \sim 1$) but not to red-shifted states ($Z_1 \sim 0$). Therefore, the structure near $E=0$ would be expected to be much larger for photoionization from the blue $n=2$ state than from the red. For comparison Fig. 7 shows the distribution of partial cross sections for excitation by π polarized light from the ground state to $E=0$ for $F=16.5$ kV/cm. The cross-section distribution is similar to that of the osillator-strength distribution for zero field (quadratic in $Z_1 - Z_2$), but enhanced for $Z_1 > Z_2$. This enhancement is due to the fact that blue-shifted final states have a larger charge density near the nucleus than red-shifted states. This new result is in qualitative agreement with weak-field results which state that red-to-red or blue-to-blue transitions are much more probable than red-to-blue or blue-to-red transitions.[10]

The enhancement can be observed easily when Fig. 8 is examined. Figure 8 gives the ionization spectrum at field values 8, 14.4, and 16.9 kV/cm, with the same polarization conditions as in Fig. 5. At the two highest fields, the 243 nm was selectively exciting the $m_l=0$ blue Stark state of the $n=2$ hydrogen state, but it was not at the field 8 kV/cm. According to the current understanding, the depth of the modulation is a slow function of the electric field; it depends on $F^{1/4}$. The fact that doubling the field from 8 to 16.9 kV/cm resulted in a change of about a factor of two in their depth underscores this effect.

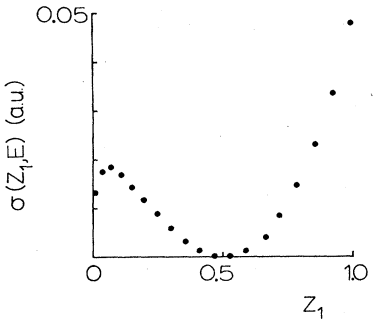

FIG. 7. The distribution of partial photoionization cross sections $\sigma(Z_1,E)$ for $E=0$ and $F=16.5$ kV/cm, for photoionization from the ground state.

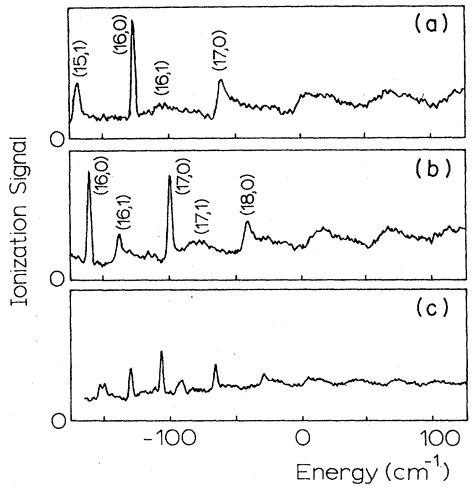

FIG. 8. The photoionization spectrum of ground state of hydrogen near $E=0$ in the presence of dc electric fields. Both beams of π polarization. In (a) and (b) the 243-nm beam is selectively exciting the $m_l=0$ blue state of $n=2$ (100). In (c) the 243-nm bandwidth is larger than the Stark splittings.

A quantitative analysis of the dependence of the depth of the Stark-induced resonances is given in Fig. 9. The raw data is given in solid circles. The data are analyzed in two different ways. In the first we use the calculated percentages of the population of the various Stark states of $n=2$ at low fields given in Fig. 2 to arrive at the depth of the modulation assuming that they were excited from the $m_l=0$ blue state alone. These reduced points are given in open circles for the field values 8, 6.5, and 4.5 kV/cm. The figure shows very good agreement between these readjusted data plus the higher field data where resolution was actually achieved, and the theoretical prediction for excitation from the pure blue intermediate state.

The same figure also gives the theoretical prediction of the depth of the modulations assuming that the Stark states of $n=2$ were never resolved at all of the applied

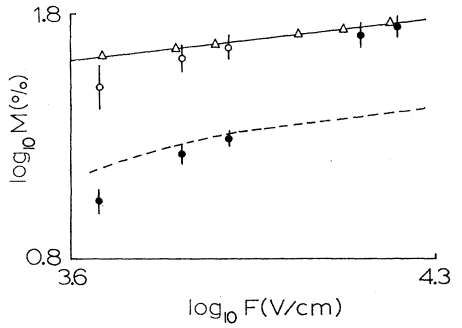

FIG. 9. The depth of the modulation at $\sim E=0$ as a function of the electric field. Solid circles are experimental points. Triangles are calculated depths assuming that the 243-nm beam selectively excited the $m_l=0$ blue state (100), and the solid line is a fit of these calculated depths. The open circles are depths derived from the low field data assuming that the laser has excited 100 blue state only (adjusted data points). The dotted curve is derived from calculations assuming the laser bandwidth is larger than the Stark splittings.

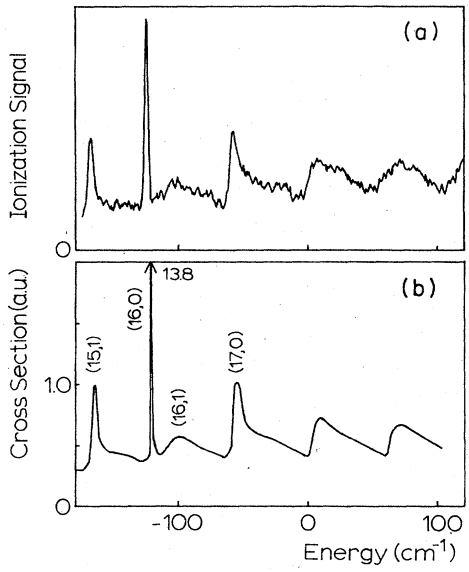

FIG. 10. Both the calculated and measured photoionization spectrum of hydrogen $m_l=0$ blue state of $n=2$ near $E=0$ at 16.7 kV/cm. The polarization of the ionizing radiation is π.

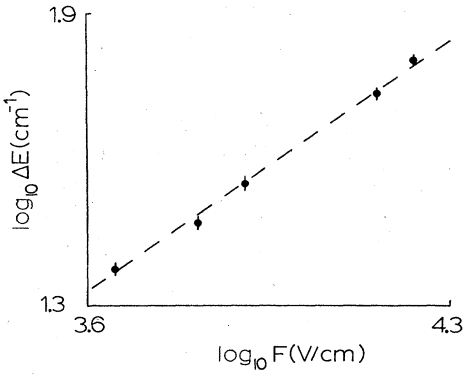

FIG. 11. Log-log plot of the experimental spacing of the resonances at $E=0$ vs field. The solid line is a least-squares fit to the form of the semiclassical formula, Eq. (28).

fields. This clearly shows the enhancement of the depth when individual parabolic states are used.

Finally, Fig. 10 gives both the measured and calculated photoionization spectrum near $E=0$ at 16.7 kV/cm with the $m_l=0$ blue state as initial state. The polarization of the ionizing beam is π. Apart from some disagreement between the heights of the sharp peak in the $E\leq 0$ region, one observes excellent agreement between the two spectra. The variation in the heights is due to the fact that the peak is very sharp (its width is dominated by the laser width) thus making the location of its true peak difficult, and subject to errors due to scan speeds. In addition, the presence of nonuniformities in the electric field in the interaction region leads to a broadening and reduction of its height.

VI. FIELD DEPENDENCE OF RESONANCE SPACING

One distinctive property of the field-induced resonances near $E=0$ is the dependence of their spacing on field. This dependence is believed to be universal; that is, the resonances for any atomic system in an electric field will obey the semiclassical formula:

$$\Delta E=(7.499\ \text{cm}^{-1})[F(\text{kV/cm})]^{3/4}\ .$$

This conclusion is based on the fact that the phase integral appearing in the quantization condition is insensitive to the behavior of the potential at small values of the coordinate. Each experimental study which has been performed on complex atoms has included a comparison between the predictions of the semiclassical formula for the threshold spacing and the experimental results. Agreement has generally been quite good, although one study reported a rather large discrepancy (7%) between the measured and theoretical values for the coefficient.[11] Since their study made use of more data points than previous studies and thus is probably the most precise test yet made of the spacing formula, their discrepancy is somewhat disturbing. Moreover, there is a competing theoretical work that predicts a $\frac{2}{3}$ power law.[12]

The best system in which to test the spacing formula is hydrogen, since the lack of core mixing and the enhancement of the resonance by excitation from pure parabolic states lead to large resonance and very good signal to background ratios. For each spectrum, the energy separation between the peak of the first resonance below $E=0$ and the peak of the second resonance above $E=0$ was measured. This value was divided by 2 to give the threshold spacing. This procedure was used to reduce the relative uncertainty in the measurement. Table II gives the results of this measurement: the first column gives the measured spacing for each field, while the second column gives the prediction of the semiclassical formula. The agreement is quite good. Figure 11 is a log-log plot of the measured spacing versus field. The solid line is the result of a linear least-squares fit of the data to the form of the theoretical formula. The resulting best-fit value for the exponent is 0.751 ± 0.02, in excellent agreement with the semiclassical result. The value for the coefficient is 7.47 ± 0.2 cm^{-1}, also in excellent agreement with the theoretical prediction. Thus, this analysis has verified the semiclassical result for the field dependence of the spacing to the highest precision reported to date.

In conclusion, we have performed measurements of the photoionization cross section of hydrogen from pure para-

TABLE II. Theoretical and experimental spacings of the resonances at threshold as a function of the electric field.

F (V/cm)	ΔE expt (cm^{-1})	ΔE semiclassical (cm^{-1})
4 500	23.7±0.6	23.2
6 500	29.5±0.7	30.5
8 000	35.6±0.8	35.7
14 400	54.5±1.5	55.4
16 900	64.0±1.5	62.5

bolic states. Such studies are not feasible in complex atoms because of the large splittings in their fine-structure components. Attempts to make measurements from higher excited states such as $n=3$ or $n=4$ are underway.

ACKNOWLEDGMENTS

This work was supported by National Science Foundation Grant No. PHY-81-09305.

---

*Permanent address: General Electric Company, Nela Park, Cleveland, OH 44112.

†On leave from the Graduate School of the University of Science and Technology of China, Beijing, People's Republic of China.

[1]D. A. Harmin, Phys. Rev. A **24**, 2491 (1981); Phys. Rev. Lett. **49**, 128 (1982); Phys. Rev. A **26**, 2656 (1982); V. D. Knodratovich and V. N. Ostrovsky, Zh. Eksp. Teor. Fiz. **4**, 1256 (1982) [Sov. Phys.—JETP **56**, 719 (1982)].

[2]R. R. Freeman, N. P. Economou, G. C. Bjorklund, and K. T. Lu, Phys. Rev. Lett. **41**, 1463 (1978); R. R. Freeman and N. P. Economou, Phys. Rev. A **20**, 2356 (1979).

[3]P. M. Koch and D. R. Mariani, Phys. Rev. Lett. **46**, 1275 (1981).

[4]W. L. Glab and M. H. Nayfeh, Phys. Rev. A **31**, 530 (1985).

[5]K. H. Welga and H. Rottke, in *Laser Techniques in the Extreme Ultraviolet—OSA, Boulder, Colorado, 1984,* edited by S. E. Harris and T. B. Lucatorto, AIP Conf. Proc. No. 119 (AIP, New York, 1984), pp. 213—219.

[6]R. J. Damburg and V. V. Kolosov, J. Phys. B **9**, 3149 (1976).

[7]E. Luc-Koenig and A. Bachelier, J. Phys. B **13**, 743 (1980); **13**, 1769 (1980); Phys. Rev. Lett. **43**, 921 (1979).

[8]W. L. Glab and M. H. Nayfeh, Opt. Lett. **8**, 30 (1983).

[9]G. Lüders, Ann. Phys. **8**, 301 (1951).

[10]H. A. Bethe and E. E. Salpeter, *Quantum Mechanics of One- and Two-Electron Atoms* (Plenum, New York, 1977), p. 276.

[11]C. Blondel, R. Champeau, and C. Delsart, Phys. Rev. A **27**, 583 (1983).

[12]I. I. Fabrikant, Zh. Eksp. Teor. Fiz. **79**, 2070 (1980) [Sov. Phys.—JETP **52**, 1045 (1980)].